

# Short wavelength electron temperature gradient instability in toroidal plasmas

Zhe Gao<sup>a)</sup>

Department of Engineering Physics, Tsinghua University, Beijing 100084, People's Republic of China

H. Sanuki and K. Itoh

National Institute for Fusion Science, Toki, Gifu 509-5292, Japan

J. Q. Dong

Southwestern Institute of Physics, Chengdu 610041, People's Republic of China

(Received 13 July 2004; accepted 5 November 2004; published online 10 January 2005)

The electron temperature gradient (ETG) driven mode in the very short wavelength region  $k_{\perp}\rho_e > 1$  is identified with a gyrokinetic integral equation code in toroidal plasmas. This “double-humped” growth rate of the conventional ETG and short wavelength ETG modes is attributed to the toroidal drift resonance mechanism and the nonmonotonic behavior of normalized real frequency as the poloidal wavelength varies. This instability provides a possibility existence of a kind of turbulence source with very small size of cells. However, the wavelength of the short wavelength ETG mode is too short and induced transport may be small unless there are inverse cascade effects. In addition, the critical threshold of electron temperature gradient  $(R/L_{Te})_c$  for the short wavelength ETG mode is higher than that for the conventional ETG mode. © 2005 American Institute of Physics. [DOI: 10.1063/1.1840709]

## I. INTRODUCTION

Short wavelength microinstabilities with a characteristic perpendicular wavelength of the order of electron Larmor radius are much less studied than its ion counterpart since it was believed that turbulence driven by such small size microinstabilities would not be able to drive a large transport. However, nonlinear gyrokinetic simulation<sup>1</sup> has shown that the turbulence driven by electron temperature gradient (ETG) instabilities can yield a large electron heat flux through radially highly elongated vortices, so called “streamers.” Experimental evidence<sup>2-4</sup> also shows that the anomalous electron transport in magnetic confined plasmas is governed by short wavelength turbulence with  $k_{\perp}\rho_i > 1$ , of course, after the suppression of long wavelength turbulence. Moreover, observation of electron temperature profile stiffness in most experiments<sup>5</sup> indicates that the short wavelength instability responsible for electron transport should have a threshold in electron temperature gradient or  $1/L_{Te} \sim \nabla T_e/T_e$ . One can also expect the linear critical temperature gradient is just same as the onset condition to excite the ETG streamers. Therefore, recent studies<sup>6,7</sup> have been performed on the ETG instabilities and the results seem to be consistent with some experimental observations.<sup>8</sup> At the same time, however, some experimental observations<sup>9</sup> seem to agree well with the model based on other instabilities, for example, the trapped electron mode–ion temperature gradient (ITG) driven mode.<sup>10</sup> Moreover, it is noted that not all tokamaks observed strong stiffness in electron temperature profile.<sup>11,12</sup> It might be attributed partly to the fact that it is difficult to separate electron and ion transport channels. However, it is also possible that the electron transport is

controlled by multisource instabilities simultaneously, or by different instability depending on different discharge condition.

Recently, new unstable modes driven by temperature gradients ( $\eta_i$  or  $\eta_e$ ) is identified by Smolyakov *et al.*<sup>13</sup> These modes represent ion and electron temperature gradient driven modes destabilized in the short wavelength regions with  $k_{\perp}\rho_{i,e} > 1$ . The ion and electron nonadiabatic response still exist due to the  $\omega_{*i,e} \propto k_{\theta}$ , which compensates for the decaying of  $I_0(b_{i,e})\exp(-b_{i,e}) \sim 1/\sqrt{2\pi}b_{i,e}$  as  $b_{i,e}$  increases at the regions  $b_{i,e} \gg 1$ , where  $k_{\theta}$  is the poloidal wave number,  $b_{i,e} = k_{\perp}^2\rho_{i,e}^2/2$  is the Larmor radius parameter, and  $I_0$  is the first-order modified Bessel function. Among them, the ion mode, we call it the short wavelength ITG (SWITG) mode, is further investigated both in slab<sup>14</sup> and toroidal<sup>15,16</sup> configuration, but the electron short wavelength mode has not identified in the toroidal geometry yet. Hirose and Elia<sup>17</sup> have reported a short wavelength electron mode, but that mode is not the short wavelength ETG (SWETG) mode discussed in Smolyakov *et al.*<sup>13</sup> In fact, the mode introduced by Hirose and Elia<sup>17</sup> is just the conventional ETG mode in the regime  $1 < k_{\perp}\rho_i \ll \sqrt{m_i/m_e}$ . If we trace that mode by increasing the  $k_{\theta}$  to about  $\rho_e^{-1}$ , we can get the conventional ETG mode. Of course, the conventional ETG mode in the regime  $k_{\perp}\rho_e \ll 1$  shows special behaviors, such as the influence of ion dynamics and the weakening of the magnetic shear stabilization effect. It is beyond our topic in this paper, for we would like to identify the SWETG mode mentioned by Smolyakov *et al.*<sup>13</sup> in the regime  $k_{\perp}\rho_e > 1$ . In principle, the SWETG mode is similar with the SWITG mode except that the roles of electrons and ions are exchanged. In our earlier works, the SWITG mode has been investigated and the physical mechanism is discussed both in slab<sup>14</sup> and toroidal<sup>16</sup> configuration.

<sup>a)</sup>Electronic mail: gaozhe@mail.tsinghua.edu.cn

In short, the slab SWITG mode is excited by the Landau (transit) resonance; and the toroidal SWITG mode is excited mostly by the toroidal drift resonance. Since the normalized frequency,  $\omega/k_{\parallel}v_{ti}$  for the slab mode and  $\omega/\omega_{Di}$  for the toroidal mode, respectively, is nonmonotonic with respect to  $k_{\theta}$ , where  $k_{\parallel}v_{ti}$  is the ion parallel transit frequency and  $\omega_{Di}$  is the ion toroidal (magnetic curvature and gradient) drift frequency. When the real frequency passes the resonance regime twice, the growth rate reveals two peaks: the first peak at  $k_{\theta}\rho_i \approx 1$  is the conventional ITG mode, and the second peak at  $k_{\theta}\rho_i > 1$  is the SWITG mode. The similar mechanism works for electron dynamics in the region  $k_{\theta}\rho_e > 1$  and one can expect the existence of the short wavelength ETG mode in the toroidal configuration. Moreover, the electron kinetics can influence the SWITG mode in the region  $k_{\perp}\rho_i > 1$ , but there is no contribution from other lighter particle at  $k_{\perp}\rho_e > 1$ . Therefore, it turns out, from the local model in shearless slab configuration,<sup>13</sup> that the SWETG cannot be stabilized at very short wavelength regions since  $k_{\parallel}$  is fixed. However, the resonance frequencies  $\omega_{De}$  for the toroidal mode, is proportional to the poloidal wavenumber in the integral model. As  $k_{\perp}$  increases large enough, the mode is expected to be stable because the resonance condition breaks down.

In this paper, we employ a set of integral eigenvalue equations for the identification and study of toroidal SWETG modes. The curvature and magnetic gradient drifts, the transit effect, and finite Larmor radius effects are retained in the model for both electrons and ions. The SWETG mode is identified and its characteristics are confirmed in this paper.

The organization of this paper is as follows. The integral eigenmode equations are presented in Sec. II. Numerical results and analyses are described in Sec. III. Section IV is devoted to conclusions and discussion.

## II. INTEGRAL EIGENMODE EQUATION FORMALISM

The ballooning representation for an axisymmetric toroidal geometry with circular flux surface is employed. The  $s$ - $\alpha$  equilibrium model is applied. The magnetic curvature and gradient drifts, the transit effect, and the finite Larmor radius effect are all retained for both ions and electrons, but the trapped particle effect is neglected.

The coupled integral eigenmode equations for low  $\beta$  plasmas are obtained from Poisson equation and the parallel component of Ampère's law as follows:<sup>16</sup>

$$\left(1 + Z_i\tau_i + \frac{k_{\perp}^2\Omega_e^2}{2\omega_p^2}\right)\phi = \sum_{j=i,e} \int_{-\infty}^{+\infty} \frac{dk'}{\sqrt{\pi}} [H_j^{00}(k,k')\hat{\phi} + H_j^{01}(k,k')\hat{A}_{\parallel}], \quad (1)$$

$$-\frac{k_{\perp}^2}{2\beta_e}\hat{A}_{\parallel} = \sum_{j=i,e} \int_{-\infty}^{+\infty} \frac{dk'}{\sqrt{\pi}} [H_j^{01}(k,k')\hat{\phi} + H_j^{02}(k,k')\hat{A}_{\parallel}], \quad (2)$$

where  $\hat{\phi}(k)$  and  $\hat{A}_{\parallel}(k)$  are the extended Fourier components in ballooning space of  $\tilde{\phi}(r)$  and  $-v_{te}\tilde{A}(r)/c$ , and

$$H_j^{00} = i\sqrt{\tau_j M_j} \text{sign}(q_j) \int_{-\infty}^0 \frac{d\tau \exp(-i\omega\tau)}{2\tau L_s \lambda_j} \times \exp\left[-\frac{(k-k')^2}{4\tau^2 L_s^2} \tau_j M_j a_j\right] \left\{ \omega \tau_j Z_j - 1 + \frac{3}{2} \eta_j - \frac{\eta_j}{\lambda_j^2} \left( \lambda_j - b_{aj} + b_{gj} \frac{I_{1j}}{I_{0j}} \right) - \frac{\eta_j (k-k')^2}{4\tau^2 L_s^2} \tau_j M_j \right\} \Gamma_{0j}, \quad (3)$$

$$H_j^{01} = \frac{-1}{2\tau L_s} (k-k') H_j^{00}, \quad (4)$$

$$H_j^{02} = \frac{1}{(2\tau L_s)^2} (k-k')^2 H_j^{00} \quad (5)$$

with

$$k = k_{\theta} \hat{s} \theta, \quad k' = k_{\theta} \hat{s} \theta',$$

$$a_j = 1 - i \frac{2\varepsilon_n \tau g(\theta, \theta')}{(\theta - \theta')} \tau_j Z_j, \quad \lambda_j = \frac{1 + a_j}{2},$$

$$g(\theta, \theta') = (\hat{s} + 1)(\sin \theta - \sin \theta') - \hat{s}(\theta \cos \theta - \theta' \cos \theta') - \frac{\alpha}{2} [(\theta - \theta') - \sin(\theta - \theta')],$$

$$\Gamma_{0j} = I_{0j} \left( \frac{b_{gj}}{\lambda_j} \right) \exp\left(-\frac{b_{aj}}{\lambda_j}\right), \quad b_{gj} = \frac{k_{\perp} k_{\perp}'}{2} \left( \frac{M_j}{\tau_j Z_j^2} \right),$$

$$b_{aj} = \frac{(k_{\perp}^2 + k_{\perp}'^2)}{4} \left( \frac{M_j}{\tau_j Z_j^2} \right),$$

$$k_{\perp}^2 = k_{\perp}^2 \{1 + (\hat{s}\theta - \alpha \sin \theta)^2\}, \quad k_{\perp}'^2 = k_{\perp}'^2 \{1 + (\hat{s}\theta' - \alpha \sin \theta')^2\}$$

$$\rho_j = \frac{v_{tj}}{\Omega_j}, \quad v_{tj} = \sqrt{\frac{2T_j}{m_j}}, \quad \Omega_j = \frac{q_j B}{m_j c}, \quad \omega_{*j} = \frac{c T_j k_{\theta}}{q_j B L_n},$$

$$L_n = -\left(\frac{1}{n} \frac{dn}{dr}\right)^{-1}, \quad \varepsilon_n = \frac{L_n}{R}, \quad \eta_j = \frac{d \ln T_j}{d \ln n},$$

$$\alpha = -q^2 R \frac{d\beta}{dr}, \quad \beta = \beta_i + \beta_e, \quad \beta_j = \frac{8\pi n T_j}{B^2},$$

$$\hat{s} = \frac{r}{q} \frac{dq}{dr}, \quad L_s = \frac{\varepsilon_n \hat{s}}{q}, \quad \omega_{pe}^2 = \frac{4\pi n e^2}{m_e}, \quad \tau_j = \frac{T_e}{T_j},$$

$$M_j = \frac{m_j}{m_e}, \quad Z_j = \frac{|q_j|}{e},$$

$q$  is the safety factor,  $I_n$  is the modified Bessel function of order  $n=0, 1$ , and  $\text{sign}(q_j)$  equals unity for electron species and minus unity for ion species. We have normalized the wave numbers  $k_{\theta}$ ,  $k$ , and  $k'$  to  $\rho_e^{-1}$ , the frequency  $\omega$  to  $\omega_{*e}$ , and the integral interval  $\tau$  to  $\omega_{*e}^{-1}$ , respectively. Also, we define  $M = M_i/1836$ ,  $Z_{eff} = Z_i$  for convenience in the following.

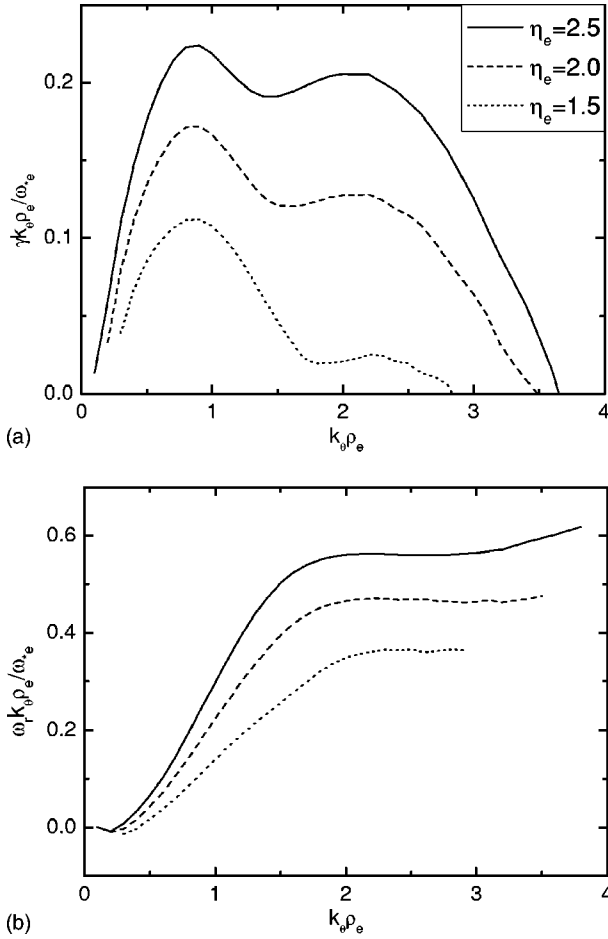


FIG. 1. Normalized growth rate (a) and frequency (b) vs  $k_{\theta} \rho_e$  for  $\tau_i = M = Z_{eff} = 1$ ,  $\hat{s} = 0.8$ ,  $q = 1.5$ ,  $\varepsilon_n = 0.1$ ,  $\beta_e = 0$ ,  $\eta_i = 2.5$ , and  $\eta_e = 2.5, 2.0$ , and  $1.5$ , respectively.

### III. NUMERICAL RESULTS AND ANALYSES

The parameters for the numerical results given here are  $\eta_e = 2.5$ ,  $\eta_i = 2.5$ ,  $\tau_i = M = Z_{eff} = 1$ ,  $\hat{s} = 0.8$ ,  $q = 1.5$ ,  $\varepsilon_n = 0.1$ ,  $\beta_e = 0$ , and  $k_{\theta} \rho_e = 2$  unless otherwise stated.

Figure 1 shows the normalized mode growth rate and frequency multiplied by  $k_{\theta} \rho_e$  vs  $k_{\theta} \rho_e$  for  $\eta_e = 2.5, 2.0$ , and  $1.5$ , respectively. Obviously, as the  $k_{\theta}$  increases, the real frequency tends to be constant and the growth rate behaves double humps: the first peak at  $k_{\theta} \rho_e \approx 1$  is the conventional ETG mode; and the second peak at  $k_{\theta} \rho_e > 1$  corresponds to the short wavelength ETG mode. In fact, the SWETG mode is rather similar to the SWITG mode we discussed in the companion work.<sup>16</sup> The physical mechanisms for these two short wavelength modes are similar except that the roles of ions and electrons are exchanged. For convenience, it is presented here in brief for the SWETG mode.

The electron density response to a fluctuating electrostatic potential is given as

$$\tilde{n}_e = \frac{-e\hat{\phi}}{T_e} n_0 + \frac{e\hat{\phi}[\omega - \omega_{*e} f(\eta_e)]}{T_e \omega - \omega_{De} - k_{\parallel} v_{te}} \Gamma_0(b_e),$$

where  $\omega_{*e} f(\eta_e)$  is the integral result of the diamagnetic drift driven by pressure gradient,  $\omega_{De} \sim \varepsilon_n \omega_{*e}$  is the toroidal (magnetic curvature and gradient) drift term, and  $k_{\parallel} v_{te} \sim v_{te} / qR$  is

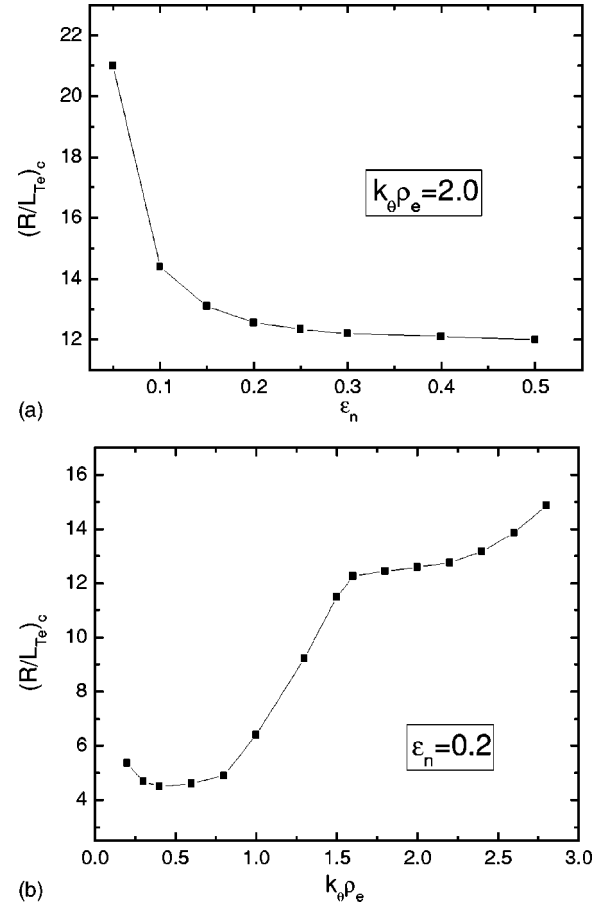


FIG. 2. Critical electron temperature scale length  $(R/L_{Te})_c$  vs  $\varepsilon_n$  for  $k_{\theta} \rho_e = 2$  (a) and vs  $k_{\theta} \rho_e$  for  $\varepsilon_n = 0.2$  (b). Other parameters are the same in Fig. 1.

the electron parallel transit frequency. Usually, the condition  $\omega_{*e} > \omega > (\omega_{De} + k_{\parallel} v_{te})$  is satisfied, so the real frequency tends to be constant due to the fact that  $\omega_{*e} = (v_{te}/L_n) \sqrt{b_e/2}$  and  $\Gamma_0(b_e) \rightarrow 1/\sqrt{2\pi b_e}$  as  $b_e \rightarrow +\infty$ . In this case, however, the resonance mechanism should be considered. In the toroidal configuration, the toroidal drift frequency is usually higher than the transit frequency. Then, the toroidal drift resonance destabilizes the toroidal mode, just like the Landau resonance in which the electron parallel transit destabilizes the slab mode. When the real frequency approaches to a critical value  $(\omega/\omega_{De})_c$ , the growth rate reached its maximum. However, the normalized frequency  $\omega/\omega_{De}$  is nonmonotonic: it increases with  $k_{\theta}$  in small  $k_{\theta}$  regions and decreases finally in large  $k_{\theta}$  regions because of  $\omega_{De} \propto k_{\theta}$ . As a result, two peaks appear in the growth rate. When  $k_{\theta}$  increases further, the condition  $\omega > \omega_{De}$  breaks down, the nonadiabatic response of electrons decays according to  $1/\sqrt{2\pi b_e}$ .

Numerical results indicate that the nonadiabatic ion response only slightly influences the conventional ETG modes in the region  $k_{\theta} \rho_e \approx 0.4$ . In the very short wavelength regime  $k_{\theta} \rho_e > 1$ , the ion contribution can be completely ignored. This is another difference between the SWITG and SWETG modes. As shown in our earlier work,<sup>14</sup> the nonadiabatic electrons will influence the SWITG mode, especially in the region  $b_i \gg 1$ , where  $\Gamma_0(b_e)$  is much larger than  $\Gamma_0(b_i)$  because  $b_e = b_i (m_e T_e / m_i T_i) < 1$ . This mechanism is especially

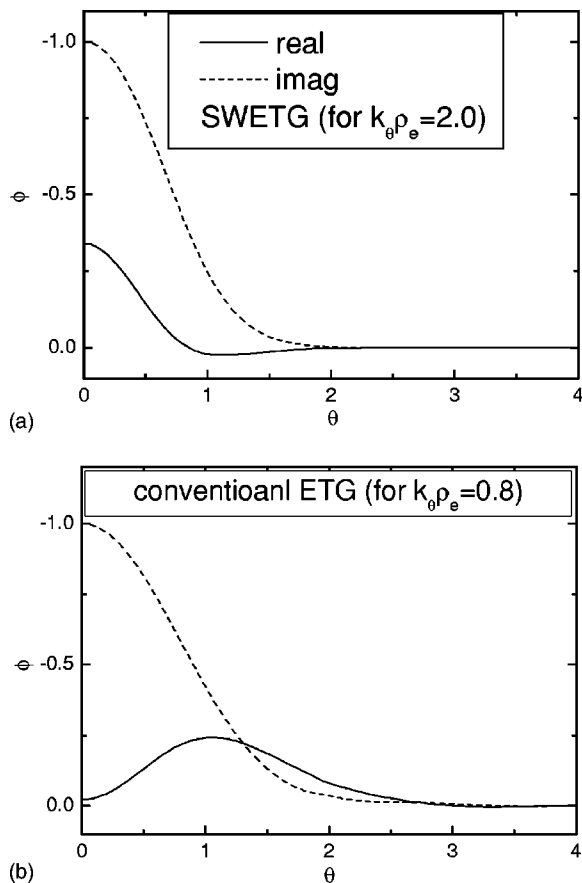


FIG. 3. Eigenfunction  $\hat{\phi}(\theta)$  for the SWETG mode at  $k_\theta \rho_e = 2$  (a) and the conventional ETG mode at  $k_\theta \rho_e = 0.8$ . Other parameters are the same as in Fig. 1.

important for the local slab mode identified by Smolyakov *et al.*<sup>13</sup> There exists no toroidal effect and the Landau resonance/damping mechanism works. Moreover, the parallel wave number  $k_\parallel$  is fixed by the local assumption. If the electrons are assumed adiabatic, the frequency and growth rate of the local slab SWITG mode tend to be constant due to the constant  $\omega_* \Gamma_0(b_i)$  in the region  $b_i \gg 1$ . But the nonadiabatic electron response strongly influences the local slab SWITG mode, which is stabilizing or destabilizing in different regions.<sup>14</sup> However, the SWETG mode is excited by the electron nonadiabatic response in the region  $k_\theta \rho_e > 1$  only, and the ion response hardly contributes the mode. As a result, the local slab SWETG mode tend to have constant frequency and growth rate, as shown in Smolyakov *et al.*<sup>13</sup>

From Fig. 1, we also can see that the SWETG mode is driven by  $\eta_e$ . The dependence of the growth rate on  $\eta_e$  is more clearly demonstrated in Fig. 2. Figure 2(a) shows the  $(R/L_{Te})_c = \eta_e / \varepsilon_n$  as functions of  $\varepsilon_n$ .  $(R/L_{Te})_c$  decreases rapidly with  $\varepsilon_n$  for  $\varepsilon_n < 0.15$  and tend to be constant for  $\varepsilon_n > 0.15$ . This character is quite similar with that of the conventional ETG mode, but the value of  $(R/L_{Te})_c$  for the SWETG mode is rather higher than that for the conventional ETG mode.<sup>6</sup> Generally, we should choose a set of  $k_\theta$  s in the fastest growing regions and find the minimum critical threshold. However, there is no explicit boundary between the conventional and short wave ETG mode. Figure 2(b) shows the

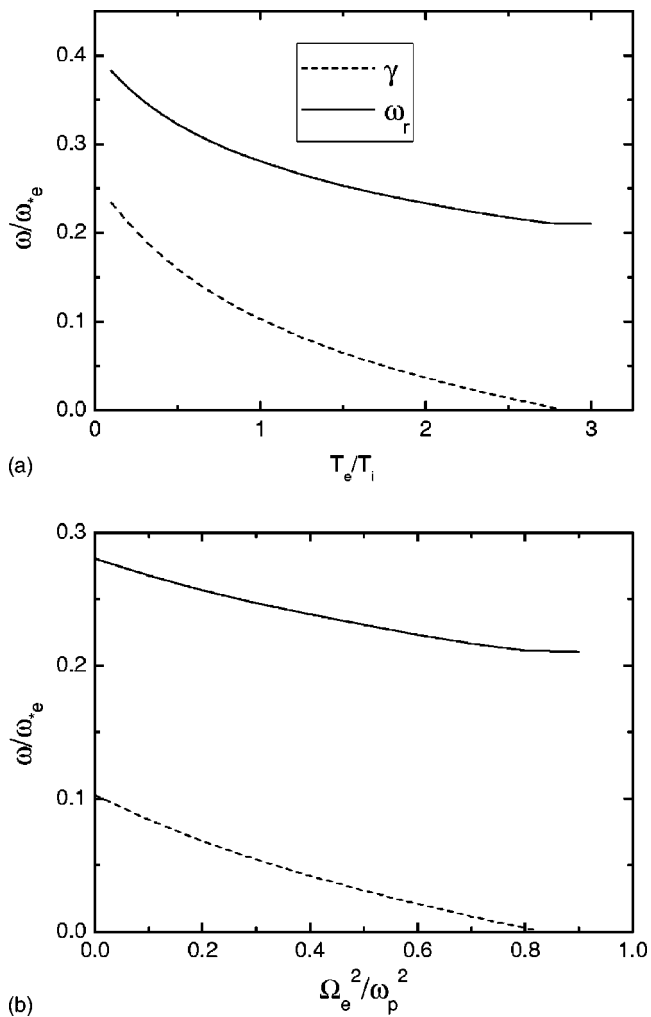


FIG. 4. Normalized frequency and growth rate vs  $T_e/T_i$  (a) and vs  $\Omega_e^2/\omega_p^2$  (b) for  $k_\theta \rho_e = 2$ . Other parameters and denotations are the same in Fig. 1.

$(R/L_{Te})_c$  vs  $k_\theta$  for  $\varepsilon_n = 0.2$ . Obviously, in the  $k_\theta$  region from 0.2 to 0.8, the minimum  $(R/L_{Te})_c$  exists with a value about 4.5, which is consistent with the results from conventional ETG mode.<sup>6,7</sup> When  $k_\theta$  increases from 0.8 to 1.6,  $(R/L_{Te})_c$  increases with  $k_\theta$  rapidly. However, it seems to be another “substeady-state” region for  $k_\theta$  from 1.6 to 2.2, where  $(R/L_{Te})_c$  is about 12.5 and slightly depending on  $k_\theta$ . When  $k_\theta$  increases further,  $(R/L_{Te})_c$  increases again.

The eigenfunctions for the short wavelength ETG mode ( $k_\theta \rho_e = 2$ ) and the conventional ETG mode ( $k_\theta \rho_e = 0.8$ ) are shown in Figs. 3(a) and 3(b), respectively. Not similar to the SWITG mode, the SWETG mode has a rather smooth and localized structure due to no ion nonadiabatic response contribution in such short wavelength regions. As the poloidal wavelength decreases, that is,  $k_\theta$  increases, the SWETG mode is more localized along the field line than the conventional ETG mode.

Figure 4 shows the normalized mode frequency and growth rate vs  $T_e/T_i$  (a) and  $\Omega_e^2/\omega_p^2$  (b), respectively. Large  $T_e/T_i (> 3)$  can stabilize the SWETG mode for the present parameters. Also, the Debye shielding effect  $\Omega_e^2/\omega_p^2$  can stabilize the SWETG more easily than the conventional ETG more, since the SWETG mode has a higher  $k_\theta$ .

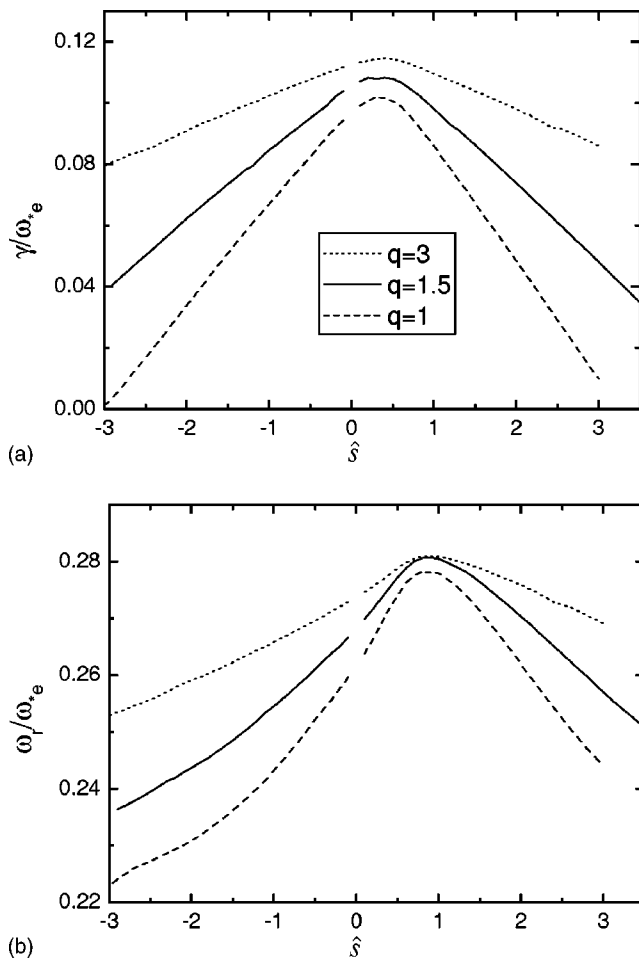


FIG. 5. Normalized growth rate (a) and frequency (b) vs  $\hat{s}$  (positive and negative) for  $k_{\theta}\rho_e=2$  and  $q=1, 1.5$ , and 3, respectively. Other parameters and denotations are the same in Fig. 1.

The magnetic shear effects are studied for both cases with positive and negative shear and the results are shown in Fig. 5. The growth rate and real frequency seems to be continuous from negative shear regions to positive shear regions, even though the case with zero shear cannot be solved from the present model. The plot of growth rate vs  $\hat{s}$  is rather symmetrical around  $\hat{s}=0.5$ . It might be explained by the dependence of the toroidal drift frequency on the magnetic shear. Since the mode is much localized in  $\theta$  space, the toroidal drift frequency  $\hat{\omega}_{De}=2\varepsilon_n\omega_{*e}[\cos\theta+\sin\theta(\hat{s}\theta-\alpha\sin\theta)]=2\varepsilon_n\omega_{*e}[1+(\hat{s}-\alpha/2)\theta^2]$ . As a result, the growth rate in negative shear regions is lower than that in positive shear regions. In addition, the stabilizing effect of magnetic shear seems to be stronger for lower  $q$  than for higher  $q$ , which is similar with the conventional ETG mode. In fact, the decrease of  $q$  increases the effective magnetic shear  $L_s=\varepsilon_n\hat{s}/q$ . However, it is noted that the results in Fig. 5 are obtained from the electrostatic model. At finite  $\beta$ ,  $q$  will influence the mode not only through the effective magnetic shear but also through the ballooning parameter, which will be discussed in the following.

Figure 6 shows the  $\alpha$  dependence of mode growth rate and frequency both for the SWETG and conventional ETG modes. Obviously, the SWETG instability is also suppressed

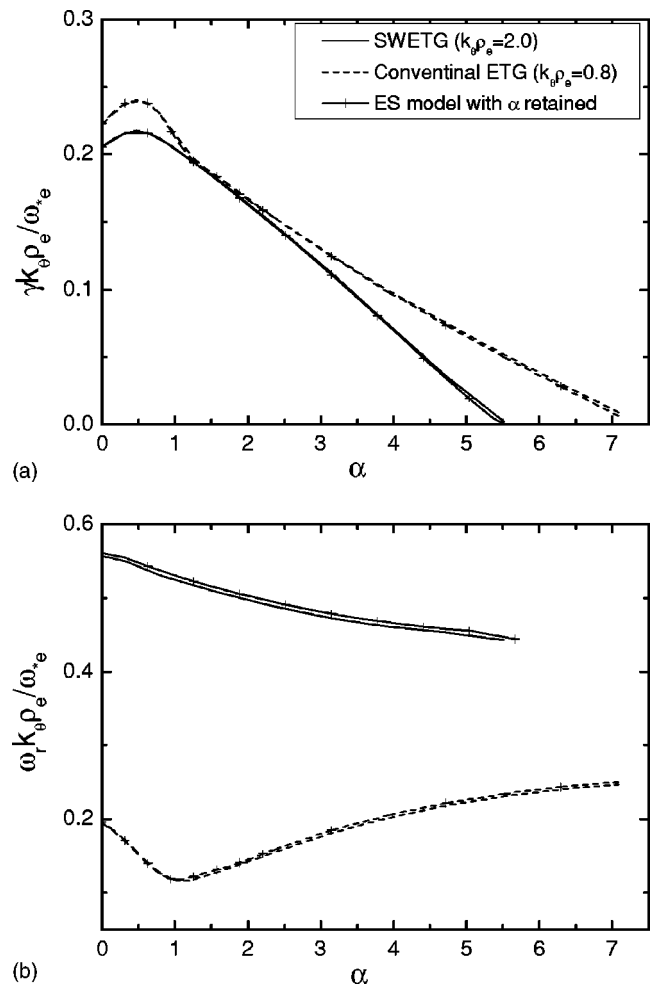


FIG. 6. Normalized growth rate (a) and frequency (b) vs  $\alpha$  for the SWETG mode at  $k_{\theta}\rho_e=2$  and the conventional ETG mode at  $k_{\theta}\rho_e=0.8$ , respectively. The lines with crosses are the results from Eq. (6) alone, but the  $\alpha$  is retained. Other parameters are the same in Fig. 1.

by  $\alpha$  and the threshold of  $\alpha$  seems to be slightly lower than that for the conventional ETG. Of course, the thresholds of  $\alpha$  for these two ETG driven instabilities are usually higher than those for ITG driven instabilities, including the conventional ITG and short wavelength ITG mode. This can be explained by the finite  $\beta$  effect. As known, the finite  $\beta$  influences the modes in the following two ways: one is the coupling to Alfvén waves; the other is the ballooning parameter  $\alpha(=-q^2Rd\beta/dr)$ . The eigenfrequency of ITG instabilities is of order  $v_{ti}/L_n$  and approaches to the frequency of sheared Alfvén waves,  $\omega_A \sim v_A/qR=v_{ti}/(qR\sqrt{\beta_i})$ . Therefore, the coupling to sheared Alfvén waves also provides a strong stabilizing effect. However, the ETG instabilities with  $\omega \sim v_{te}/L_n$  is hardly influenced by the coupling effect to sheared Alfvén waves. Figure 6 also shows the results from the electrostatic model, Eq. (1) alone, however, with the effect of  $\alpha$  retained. These results are almost the same as those from the finite  $\beta$  model.

Due to the  $\alpha$  stabilization effect, dependence of the mode frequency on some parameters shows different behaviors between the electrostatic case and the finite  $\beta$  case. Figure 7 shows the mode frequency as functions of  $\eta_i$  and  $q$  for

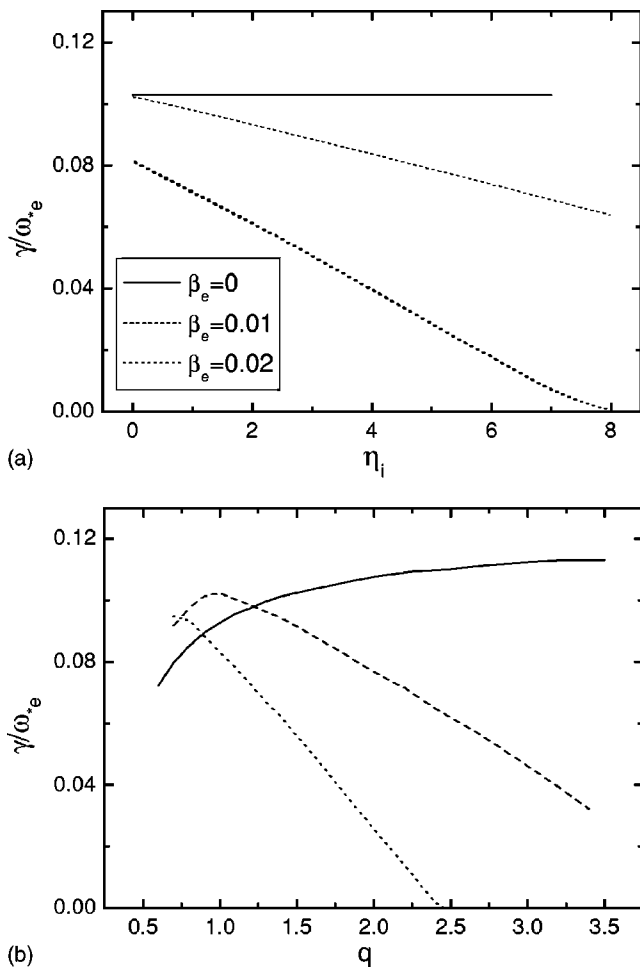


FIG. 7. Normalized growth rates vs  $\eta_i$  (a) and  $q$  (b) for  $k_\perp \rho_e = 2$  and  $\beta_e = 0, 0.01, \text{ and } 0.02$ , respectively. Other parameters and denotations are the same in Fig. 1.

$\beta_e = 0, 0.01, \text{ and } 0.02$ , respectively.  $\eta_i$  offers no contribution in the electrostatic case, but is stabilizing at finite  $\beta$  since  $\alpha (= (q^2 \beta_e / \varepsilon_n) [1 + \eta_e + (1 + \eta_i) / \tau_i])$  increases with  $\eta_i$ . Similarly, the growth rate for  $\beta = 0$  tends to be constant in large  $q$  regions because the electron parallel transit effect becomes rather small, while a large  $q$  can stabilize the mode at finite  $\beta$  through  $\alpha$  stabilization.

Figure 8 shows the dependence of growth rate and real frequency on  $\varepsilon_n$  for  $\beta_e = 0, 0.01, \text{ and } 0.02$ . In the low  $\varepsilon_n$  region, the normalized growth rate increases with  $\varepsilon_n$ , which implies the toroidal driving effect. However, the SWETG mode becomes stable at not very large  $\varepsilon_n (> 0.19)$ , where the conventional ETG persists unstable. It is because the nonadiabatic electron response decays after the  $\omega_{De}$  increases so much that the condition  $\omega > \omega_{De}$  is broken. The influence of  $\beta$  on the effect of  $\varepsilon_n$  seems to be different from the effect of  $\eta_i$  or  $q$ . It might be understood from the expression of  $\omega_{De}$ , where  $\varepsilon_n$  exists in two terms with opposite signs.

#### IV. CONCLUSIONS

The electron temperature gradient driven mode in the very short wavelength region,  $k_\perp \rho_e > 1$ , is identified with a gyrokinetic integral equation code in toroidal plasmas. This

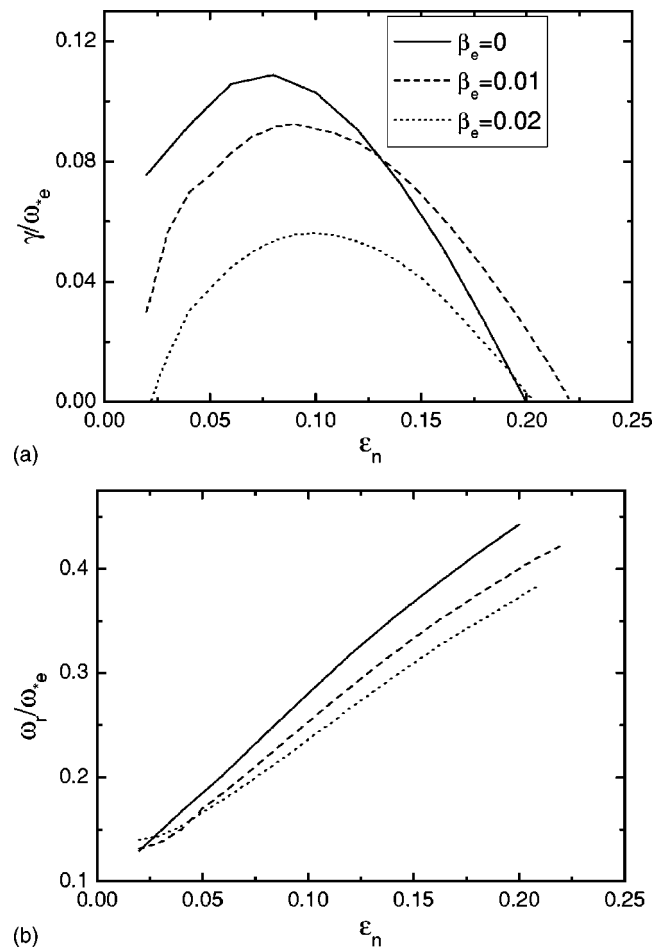


FIG. 8. Normalized growth rates (a) and real frequency (b) vs  $\varepsilon_n$  for  $k_\perp \rho_e = 2$  and  $\beta_e = 0, 0.01, \text{ and } 0.02$ , respectively. Other parameters and denotations are the same in Fig. 1.

mode propagates in the electron diamagnetic direction and seems to be a continuous extension of the conventional ETG mode. This instability occurs due to the nonadiabatic electron response in the region  $k_\perp \rho_e > 1$ , so it might be the toroidal mode from the integral code corresponding to the slab mode with the local ( $k_\parallel = \text{const}$ ) assumption by Smolyakov *et al.* However, the toroidal drift resonance is dominant in the toroidal configuration. When the normalized real frequency  $\omega/\omega_{De}$  approaches to a critical value, the growth rate reached its maximum. Therefore, the nonmonotonic behavior of  $\omega/\omega_{De}$  with respect to  $k_\theta$  results in the “double-humped” growth rate: the conventional ETG mode and the SWETG mode. This mechanism is quite similar to that for short wavelength ITG mode except that the roles of ions and electrons are exchanged and that the ion response hardly contributes the short wavelength ETG mode.

The short wavelength ETG mode is excited when  $\eta_e$  exceeds the threshold. In the region near  $k_\perp \rho_e \sim 2$ , the short wavelength ETG mode provides a quasisteady threshold  $(R/L_{Te})_c \sim 12.5$  for typical parameters. However, this threshold is larger than that from the conventional ETG mode. Dependence of the mode stabilization property on other parameters has also been investigated. The short wavelength ETG mode can be stabilized by strong magnetic shear, tem-

perature ratio, Debye shielding effect, and finite  $\alpha$ . It seems that the short wavelength ETG mode is quite similar and more stable than the conventional ETG mode. In addition, the wavelength of the short wavelength ETG mode is much shorter and induced transport may be smaller unless there is inverse cascade effects. However, the study of the short wavelength ETG mode indicates the existence of a kind of turbulence source with very small size of cells. On the other hand, the investigation of short wavelength ETG instability also indirectly identifies the short wavelength ITG instability due to the similar mechanism. The latter might be important since the short wavelength ITG mode has intermediate wavelength between  $\rho_e$  and  $\rho_i$  and might induce a high level transport.<sup>16</sup>

## ACKNOWLEDGMENTS

One of the authors (Z.G.) is grateful for the hospitality by many staff members during his visit at the National Institute for Fusion Science, Japan. His work was supported by the Visiting Professorship from Japanese Ministry of Education, Science, and Culture and by the Improving Tsinghua to Top-ranking University Fund. This work was also partly supported by the National Natural Science Foundation of China (NSFC) grant Nos. 10405014 and 10135020.

<sup>1</sup>F. Jenko, W. Dorland, M. Kotschereuther, and B. N. Rogers, *Phys. Plasmas* **7**, 1904 (2000).

- <sup>2</sup>G. D. Conway, D. N. Borba, B. Alper *et al.*, *Phys. Rev. Lett.* **84**, 1463 (2000).
- <sup>3</sup>K. L. Wong, N. L. Bretz, T. S. Hahm, and E. Synakowski, *Phys. Lett. A* **236**, 339 (1997).
- <sup>4</sup>C. M. Greenfield, K. H. Burrell, T. A. Casper *et al.*, *Proceeding of 27th EPS Conference on Controlled Fusion and Plasma Physics, Budapest 2000*, edited by K. Szegő, T. N. Todd, and S. Zoletnik (European Physical Society, Petit-Lancy, 2000), ECA Vol. 24B, p. 544.
- <sup>5</sup>F. Ryter, C. Angioni, M. Beurskens *et al.*, *Plasma Phys. Controlled Fusion* **43**, A323 (2001).
- <sup>6</sup>J. Q. Dong, G. D. Jian, A. K. Wang, H. Sanuki, and K. Itoh, *Nucl. Fusion* **43**, 1185 (2003).
- <sup>7</sup>F. Jenko, W. Dorland, and G. W. Hammett, *Phys. Plasmas* **8**, 4096 (2001).
- <sup>8</sup>W. Horton, G. T. Hoang, C. Bourdelle *et al.*, *Phys. Plasmas* **11**, 2600 (2004).
- <sup>9</sup>F. Ryter, G. Tardini, F. De Luca *et al.*, *Nucl. Fusion* **43**, 1936 (2003).
- <sup>10</sup>H. Nordman, J. Weiland, and A. Jarmen, *Nucl. Fusion* **30**, 983 (1990).
- <sup>11</sup>J. C. DeBoo, M. E. Austin, R. V. Bravenc *et al.*, *Proceeding of 29th EPS Conference on Controlled Fusion and Plasma Physics, Montreux 2002*, edited by R. Behn and C. Varandas (European Physical Society, Petit-Lancy, 2002), ECA Vol. 26B, p. 2064.
- <sup>12</sup>W. Suttrop, R. Budny, J. G. Cordey *et al.*, *Proceeding of 28th EPS Conference on Controlled Fusion and Plasma Physics, Funchal 2001*, edited by C. Silva, C. Varandas, and D. Campbell (European Physical Society, Petit-Lancy, 2001), ECA Vol. 25A, p. 989.
- <sup>13</sup>A. I. Smolyakov, M. Yagi, and Y. Kishimoto, *Phys. Rev. Lett.* **89**, 125005 (2002).
- <sup>14</sup>Zhe Gao, H. Sanuki, K. Itoh, and J. Q. Dong, *Phys. Plasmas* **10**, 2831 (2003).
- <sup>15</sup>A. Hirose, M. Elia, A. I. Smolyakov, and M. Yagi, *Phys. Plasmas* **9**, 1659 (2002).
- <sup>16</sup>Z. Gao, H. Sanuki, K. Itoh, and J. Q. Dong, *Phys. Plasmas* **12**, 022502 (2005).
- <sup>17</sup>A. Hirose and M. Elia, *Phys. Plasmas* **9**, 4664 (2002).